

Numerical simulation of dust event during (1-6) June 2012 using BSC-DREAM8b dust regional model over West Asia, a case study

Sama K. Mohammed¹, Neamah M. Al Fatla², Saadi A. Abdul Wahab³

1, 2, 3 Department of Atmospheric Sciences, College of Science, AL-Mustansiriyah University, Baghdad, Iraq

Abstract: Sand and Dust Storms (SDS) are a major problem and Iraq is considered one of the affected countries in the Middle East, facing an increment in the frequency and intensity of extreme weather events, especially SDS. The BSC-DREAM8b v2.0 model was used to simulate dust outbreak for West Asia centered over Iraq for the period (1-6) June 2012 which was intense and considered as natural hazard. To evaluate the performance of the model, quantitative and qualitative evaluations were done to verify the performance of the BSC-DREAM8b model as weather and dust forecasting tool by using ERA-I reanalysis, Ground-based and space-borne observations data. Also the source mask was used to cover the region below 35° N latitude (SM35) and then it was extended to cover the region below 45° N latitude (SM45).

The model shows its ability in simulating the synoptic patterns reasonably well over the region of study for all the tested days, predicted the dust event successfully and simulated well the movement of the dust plume with underestimated values for the Dust Optical Depth (DOD) by using both types of extended source masks, compared to Aerosol Optical Depth (AOD) for Solar_Village AERONET site, and with zero values when the dominated aerosols are from fine mode. The model succeeded in simulating the activation of dust sources in Syria, Iraq, areas in Kuwait, UAE, Iran and eastern KSA but it missed out the activation of dust sources in southern KSA. Compared to MODIS AOD, DOD values were underestimated in which AOD includes all types of aerosols while the model computed dust only. Using the source mask SM45 improved the values of the DOD and gave higher values with the same behavior.

Keywords: AERONET, aerosol optical depth, dust storms, mineral dust, dust forecasting.

I. Introduction

Mineral dust loading in the atmosphere is the most abundant of all aerosol species together with sea-salt aerosol in some coastal areas [1]. Dust is the most important aerosol by mass compared to soot from natural fires, sulphates from industrial exhaust, ash from volcanic eruptions and sea salt [2]. Mineral dust is a mixture of carbonates, sulphates, organic material and soot particles [3]. The main driver of dust emissions is wind, in addition to the surface characteristics which play a key role for their spatial distribution, intensity and frequency.

West Asia including Arabian Peninsula, Syria, Iraq and Iran has been recognized as one of the most important primary sources of dust [4], [5]. In addition to natural dust sources which are globally account for 75% of emissions, there are anthropogenic sources which account for 25% with largest observed sources in Mesopotamia and Saudi Arabia [6] in which dust sources is observed over the Empty Quarter (or Al-Rub' Al-Khali desert) considered as one of the largest sand deserts in the world that occupies much of the southern interior of the Arabian Peninsula and it is connected to the An Nafud sand sea in the north by the Ad-Dahna, a sand corridor and central Saudi Arabia. The Arabian Peninsula affected by dust from Tokar Gap in north-eastern Sudan, near the Red Sea in summer season. South-western Iran and areas on the Iranian coast of the Arabian Gulf are also active dust sources. In general under different synoptic and mesoscale weather conditions, most of the region (apart from Turkey) is a potential dust source [7].

The emitted dust can not only impact the area surrounding its origin, but can also impact land and people at great distance away where the dust finally settles. Due to the frequent occurrence of dust storms over desert dust sources in North Africa and Middle East, the impacts of the problem are on different sectors such as health, aviation, marine navigation, agriculture, water resources (due to the dust deposition in rivers and water reservoirs), and climate, thus it became very urgent to have an accurate prediction of dust storm over the region.

Models of dust emission, transport and deposition are used as a tool to understand the various aspects that control distributions and impacts of dust. Regional dust models are the ideal tool to study in detail the processes that influence dust distribution as well as individual dust events. While global models are used to investigate dust at large scales and long term changes.

Compared to central and western Africa, eastern Africa and the Arabian Peninsula have relatively few available in situ observations and modeling studies. The Earth Sciences Department at Barcelona Supercomputing Center (BSC) maintains dust forecast operations with the updated version of the former Dust Regional Atmospheric Model (DREAM) [8] called BSC-DREAM8b [9], [10], [11] and conducts modeling research and developments for short-term prediction.

Pérez et al. (2006) [9], [10] analyzed the BSC-DREAM8b model in terms of AOD from AERONET sunphotometers and satellite images for two dust events during April and June 2002 which affects the Western Mediterranean region. The results emphasize the capability of the model to correctly reproduce the timing increase of the observed dust peaks in that region. Moreover, the inclusion of dust radiation interactions improved significantly the temperature and mean sea-level pressure forecasts over dust-affected areas.

Haustein et al. (2009) [12] evaluated the BSC-DREAM8b by comparing the model outputs with the dust dataset from SAMUM 2006 field campaign. He obtained a fairly good agreement between model results, AERONET data, and satellite observations with respect to their horizontal and vertical distribution. Papanastasiou et al. (2010) [13] evaluated the BSC-DREAM8b model in Greece using model PM10 predictions covering a 7-year period (2001-2007). The results indicated that dust regional modeling can be regarded as a useful tool for air quality managers when assessing compliance with air quality limit values.

Pay et al. (2010) [14] and Basart et al. (2012) [15] evaluated the BSC-DREAM8b model for the year 2004 in the framework of the CALIOPE air quality system which provides air quality forecast for Europe (12km x 12km) and Spain (4km x 4km). For the European domain, they used daily PM10, PM2.5 and aerosol components data from 55 stations of the EMEP/CREATE network and total, coarse and fine aerosol optical depth (AOD) data from 35 stations of the AERONET sun photometer network. The results showed that overall PM and AOD levels are underestimated by CALIOPE, the higher correlations of the PM10 and the coarse mode AOD were largely due to the accurate representation of the African dust influence in the forecasting system by means the inclusion of the BSC-DREAM8b model outputs. While for the Spanish domain, Pay et al. (2012) [16] used a new data set of Saharan dust PM10 concentration to evaluate the PM10 contribution modelled by BSC-DREAM8b and they found that the BSC-DREAM8b was able to reproduce the daily variability of the observed levels of desert dust and most of the outbreaks affecting southern. Basart et al. (2012) [15] compared the BSC-DREAM8b outputs with AERONET observations for the year 2004. The results shows that the model reproduces correctly the long-range transport towards Europe and North Atlantic regions but it underestimates the dust load in the Sahel and the Eastern Tropical North Atlantic regions in winter and spring. While it overestimates the dust load in Middle East in summer as well as in Northern Algeria and the dust transport towards the Western and Central Mediterranean mainly in spring.

This work aims to evaluate quantitatively and qualitatively the performance of the BSC-DREAM8b model as a weather and dust forecasting tool over west Asia region centered over Iraq, this will lead to compensate the lack in dust observations such as Dust Optical Depth (DOD) over the region of study.

This contribution include the characterization of the synoptic patterns that lead to dust emission by analyzing the surface and upper air charts at 850 hPa, wind speed, and evaluate the results by comparing them with ERA-I reanalysis data, then comparing the simulated dust optical depth DOD with measurements from ground-based and space-based instruments. The chosen dust outbreak case was intense and considered as natural hazards according to the Earth Observatory website: (<http://earthobservatory.nasa.gov/IOTD/view.php?id=78170>).

The paper is organized as follows. Section II describes the BSC-DREAM8b dust forecasting system, section III describes the methodology including the model configurations, the observational data used in evaluating the model. Section IV includes the discussion of the results and finally conclusions are included in Section V.

II. Bsc-Dream8b V2.0 Dust Forecast System

The BSC-DREAM8b v2.0 forecast system divided into three main parts which in turn consist of several subsystems: Pre-Processing, Model Operational System and Post-Processing.

Pre-processing: it is a set of routines required to prepare input data to the model grid. Its functions include two parts: the set-up which includes the definition of simulation domains and model configuration and the interpolation of terrestrial data (such as terrain, land use, and soil types) and sea surface temperature (SST) to the simulation domain, and the pre-processing of the model which includes a download, degrib and interpolation of the meteorological input data (H, U, V and Q) from the global meteorological model to the simulation domain, as well as, the initial and boundary conditions for the dust model.

Model operational system: it is composed of numerical integration programs of the BSC-DREAM8b v2.0 core which was designed to predict the dust cycle of the eroded desert dust in the atmosphere and it consist of two parts: the atmospheric modeling system and the dust cycle module. The atmospheric modeling system is NCEP/Eta model [17], [18], [19] uses the primitive equations based on the hydrostatic approximation which is formulated as a grid-point model and the partial differential equations are represented by finite-difference schemes [17]. In the horizontal, the prognostic meteorological variables were distributed on the semi-staggered Arakawa E grid showing a good performance in simulating smaller-scale processes (such as gravity-inertia disturbances). The method, which provides a proper behavior of the model with variables on the E grid, is developed for strong physical forcing (e.g. orography influence, convection, turbulence). In the vertical, the

step-mountain Eta (η) vertical coordinate was used. It leads to quasi-horizontal coordinate surfaces which prevents the error of pressure-gradient force due to steep topography that can occur with terrain-following coordinates (σ). The dust cycle module simulated through the concentration equation [8] and it includes schemes of dust emission (source), transportation and dust deposition (sink). The BSC-DREAM8b v2.0 model solves the Euler-type partial differential non-linear equation for dust concentration as an additional component into the NCEP/Eta model. Eulerian-type transport models are able to represent all major phases of dust life cycle [20]. Post-Processing: it includes the GrADS and NetCDF outputs files with the conversion from E-Arakawa grid to georeference grid and the maps generation process.

2.1 Emission Scheme:

In order to determine whether the soil particles can be uplifted, some factors should be specified which are related to land-surface nature, the physical properties of the soil particles such as soil texture, moisture, particle cohesiveness and particle size distribution as well as surface wind speed and the threshold velocity of wind erosion [21]. Dust source function includes data sets about the type of vegetation represented by the source mask (desert mask), the type of soil and the inclusion of the preferential source mask.

The BSC-DREAM8b v2.0 model calculate the source mask term (S) from remapping the arid and semiarid categories of the global United State Geological Survey (USGS) vegetation dataset to the regional model domain, this data has a spatial resolution of 30 seconds of arc (1 km at the equator) and include 100 vegetation types which then transformed into 13 SSiB vegetation types [22]. To characterize soil texture classes required by the NCEP/Eta model, two datasets were used: the Staub and Rosenzweig Zobler near-surface global soil texture (referred to as ZOBLER) at 1° resolution [23] and the UNEP/GRID gridded FAO/UNESCO soil units is used (referred to as FAO) [24]. The global dataset has a spatial resolution of 2 minutes in a regular latitude/longitude grid (approximately 4km at the equator). The different FAO soil types are transformed into 9 Zobler types, for each 9 types the fractions of clay, small silt, large silt, and sand were estimated from texture triangle [25]. The parameterization scheme of the NCEP/Eta model required information on the soil types, thus soil types according to Cosby et al (1984) [26] were corresponded to the Zobler texture classes. Also the BSC-DREAM8b v2.0 model included a preferential source mask from Ginoux et al. (2001) [27] in which the preferential sources and the seasonal changes in vegetation cover were incorporated in an explicit way whereas other models of dust cycle allow vegetation type to implicitly or explicitly influence dust sources but are not taking into account seasonal variations in vegetation cover and their impact on dust source areas [21].

The total mass of injected dust strongly depends on particle size distribution [8]. The BSC-DREAM v2.0 model included the bin method used by Tegen and Lacis in which clay and small silt are divided into eight bins [9] within the interval (0.1-10) μm radius in which it have the most significant effects on solar radiation, and the model use a mass size distribution at sources derived from D'Almeida's (1987) [28].

The BSC-DREAM8b v2.0 model dust emission scheme parameterizes the vertical dust flux F_k for each particle bin K following Shao et al. (1993) [29]:

$$F_k = C_t S \beta_k \gamma_k u^3 \left[1 - \left[\frac{u_{*ik}}{u} \right]^2 \right] \quad \text{For } u_* \geq u_{*ik} \quad (1)$$

Where

C_t is a constant tuning parameter

u_* is the friction velocity

u_{*ik} is the threshold friction velocity above which dust production starts

S is the source term (which includes the desert mask)

β_k is the fraction of each texture class of bin K and includes the influence of soil textures

γ_k is the ratio of the mass available for uplift and the total mass of the respective bin K

The threshold friction velocity of the dry soil u_{*ikd} according to Bagnold (1941) [30] is direct proportional with the particle size, neglecting cohesive forces among small particles:

$$u_{*ikd} = A_k \sqrt{2 g r_k \frac{\rho_k - \rho_a}{\rho_a}} \quad (2)$$

Where

g is the gravity acceleration

r_k is the particle radius size

ρ_k is the density of the particle

ρ_a is the density of ambient air

A_k is a function of the particle Reynolds number

$$(Rr)_{\rho k} = (2r_k u_{*ik}) / V \tag{3}$$

Where $V = 0.000015 \text{ m}^2/\text{s}$ and specified by using available empirical data [31].

Also the BSC-DREAM v2.0 model included the influence of soil structure and particle size distribution in the emission scheme by means of S , β_k and ρ_k .

Soil moisture can inhibit dust emission by increasing the threshold friction velocity of soil particles, thus the model included this effect following Fecan et al. (1999) [32]:

$$u_{*ik} = u_{*ik} \sqrt{1 + 1.21(w - w')^{0.68}} \tag{4}$$

Where

w is the ground wetness predicted by the model

w' is the amount of adsorbed water which is an increasing function of the clay fraction in the soil in which

$$w' = 0.0014(\%Clay)^2 + 0.17(\%Clay)$$

2.2 Deposition scheme

Dust particles experience removal processes during their transportation which control their lifetime in the atmosphere and hence their radiative effects. They can be removed by either dry deposition or wet deposition. In general, dry deposition is the dominant process in the vicinity of source regions due to the presence of large dust particles and also due to the dry climate prevailing in deserts. While far from the source regions, wet deposition is usually the dominant removal process for dust particles [33]. Based on Zhang et al. (2001)[34], the parameterization of dust dry deposition at the bottom layer of the model use simplified empirical parameterizations for deposition processes of Brownian diffusion, impaction, interception and gravitational settling detailed in Slinn (1982)[35]. The dry deposition of larger particles is controlled by sedimentation (or gravitational settling) and is therefore less sensitive to surface properties. The BSC-DREAM8b v2.0 model includes a simple wet scavenging scheme which uses a basic precipitation model with a constant washout ratio. The deposition on the surface (below cloud scavenging) is calculated by (Nickovic et al., 2001) [8].

2.3 Dust-Radiation Scheme

BSC-DREAM8b v2.0 model treated dust as a radiatively active substance interact with short and long wave radiation in which particle size distribution considered as one of the key factors in dust interactions. Within each transport bin, dust is assumed to have time-invariant, sub-bin log-normal distribution [36] employing the transport mode with mass median diameter of 2.524 μm [37] and a geometric standard deviation of 2.0 [38]. Physical and optical properties were accurately prescribed within this sub-bin distribution. For each size bin and wavelength the calculations of the extinction efficiency, single-scattering Albedo and asymmetry factor were made with a Mie-algorithm based on the work of Mishchenko et al. (2002) [39] assuming that each particle is homogeneous and spherical. Nonsphericity of desert dust can result in significantly different scattering properties than those predicted by Mie theory [40] while its effect upon radiative fluxes and Albedos is small [41].

The Aerosol optical depth and the extinction coefficient are related to column mass loading and mass concentration, respectively, by:

$$\tau(\lambda) = \sum_1^8 \tau_k(\lambda) = \sum_1^8 \frac{3}{4\rho_k r_k} M_k Q_{ext}(\lambda)_k \tag{5}$$

$$a(\lambda) = \sum_1^8 a_k(\lambda) = \sum_1^8 \frac{3}{4\rho_k r_k} C_k Q_{ext}(\lambda)_k \tag{6}$$

Where:

$\tau_k(\lambda)$ is the AOD for each size bin K,

$a_k(\lambda)$ is the extinction coefficient for each size bin K

ρ_k is the particle mass density

r_k is the effective radius for each size bin K

M_k is the column mass loading for each size bin K

C_k is the concentration for each size bin K

$Q_{ext}(\lambda)$ is the extinction efficiency factor.

III. Methods

The methodology used in this study consists of three parts: the first part is the set up of the BSC-DREAM8b model with a certain configuration convenient to the area of study in order to simulate the dust event. The second part is to characterize the synoptic patterns that lead to dust emission which include the surface and upper air charts at 850 hPa, 10m wind speed and direction, and evaluate the results with ERA-I reanalysis data. The third part is to follow the trajectory of dust plumes and to test the performance of the model by evaluating the results with dust measurements from ground-based and space-based instruments.

3.1 Model configuration

In order to simulate the dust event, the BSC-DREAM8b v2.0 model diagnosis has been performed for West Asia region centered over Iraq extended from 24° to 40° N latitudes and 34° to 60°E longitude, with 24h forecasts of each day with outputs for forecast every 3h and number of Grid Points IM, JM of 46 x 67. The preferential source mask was used to cover the region below 35° N latitude and then it was extended to cover the region below 45°N. Table (1) summarizes the model components and configurations.

3.2 Reanalysis outputs

To evaluate the model by means of meteorological fields and spatial patterns, the European Centre for Medium-Range Weather Forecast (ECMWF) ERA-Interim (ERA-I) Reanalysis outputs were used. They are the latest global atmospheric reanalysis produced by ECMWF as a transition between ERA-40 and a future reanalysis project. they provide information on a large variety of surface parameters (3-hourly), describing weather as well as ocean-wave and land-surface conditions and 6-hourly upper-air parameters (37 pressure levels up to 1 hPa) on a 0.25° × 0.25° grid.

Table (1) Model descriptions, components and configurations

Model	BSC-DREAM8b v2.0
Institution	BSC - CNS
Meteorological Drive	Eta/NCEP
Meteorological initial fields	FNL/NCEP (1°x1°) at 00 UTC at intervals of 6 hours
Source mask	USGS-FAO with Ginoux et al. (2001)[27]
Emission scheme	Uplifting (Shao et al.(1993)[29]; Janjic (1994)[18]; Nickovic et al.(2001)[8])
Deposition schemes	Dry deposition (Zhang et al. (2001) [34]and below-cloud scavenging (Nickovic et al. (2001)[8])
Sedimentation scheme	Gravitational settling (Zhang et al. (2001)[34])
Horizontal resolution	1/3° x 1/3° in Arakawa E-grid
Vertical resolution	24 Eta-layers in the troposphere (~15km)
Height first layer	86 m (above sea level)
Radiation interactions	Yes
Transport size bins	8 bins (0.1– 10 µm) Tegen and Lacis (1996)[42]

ERA-I uses an improved atmospheric model and a more sophisticated data assimilation method (4D-Var) for atmospheric analysis compared to ERA-40. Reanalysis data provide a multivariate, spatially complete, and coherent record of the global atmospheric circulation. Unlike archived weather analyses from operational forecasting systems, a reanalysis is produced with a single version of a data assimilation system including the forecast model used and is therefore not affected by changes in method [43].

3.3 Ground-based observations data

The AERONET (AErosol RObotic NETwork) [44] is a federation of ground-based remote sensing aerosol networks consists of sun and sky scanning spectral Cimel robotic sun photometers that automatically measure the intensity of sunlight and directional sky brightness from the UV (340 nm) to the near infrared (1640 nm) in nine spectral band passes throughout the day. These data are relayed by satellite or FTP connection to NASA's Goddard Space Flight Centre (GSFC) or through PHOTONS (photométrie pour le traitement opérationnel de normalisation satellitaire), where they are processed in near-real-time (NRT) to retrieve AOD, particle-size distribution and complex index of refraction data available through the public access website: <http://aeronet.gsfc.nasa.gov>. Aerosol optical depth data are computed for three data quality levels: Level 1.0 (unscreened), Level 1.5 (cloud-screened) and Level 2.0 (cloud-screened and quality-assured). The other AOD-dependent products are derived from these levels and may implement additional quality checks. Version 2 AOD processing now includes fine and coarse mode AOD as well as fine mode fraction. The dataset constitute a high-quality with low uncertainty (0.01–0.02) and high temporal resolution (15 min) under cloud-free conditions [44] with higher error in the UV wavelength [45], this is due to the standardization of instruments, calibration,

processing and distribution for the network. Thus the dataset has been widely used in aerosol research and characterization, validation of satellite retrievals, and evaluation of the models performance but it have limited spatial coverage although it's high time resolutions, for example in west Asia region, Iraq and the some of its neighbors are not connected to this network such as Jordan, Syria while there are few stations in Saudi Arabia and Iran.

For the validation of the model performance, a quantitative comparison has been made between the modeled optical data in the mid-visible spectrum at 550 nm and AERONET observations which obtained for level 2.0 from data between 440 and 870 nm following the Angstrom's law in order to use the same mid-visible spectrum. On average, the AERONET data are acquired at 15-minute intervals, in order to use this data for the comparison with the model outputs; all AERONET measurements within ± 90 minutes of the model three hourly outputs were extracted.

Because of the presence of different types of aerosols mixed with dust in the measurements, Angstrom exponent ($\alpha_{440 - 870}$) has been used since it is considered as a good indicator of the dominant size of the atmospheric particles. Lowest values of Angstrom parameter are associated to large particles, in which the extinction doesn't have spectral dependency, whereas the highest values are associated to the fine particle presence, whose scattering has a strong spectral dependency. In general, for increasing of the Angstrom parameter which is due to influence of anthropogenic pollutants (which are not considered in the BSC-DREAM8bv2.0 model), the modeled DOD compared to AOD from Sun-photometer tends toward under prediction [10].

Three stations have been used which are distributed on the specified domain according to the availability of data for the timing of the case study, and they are listed in Table (2) and their locations are demonstrated on a map in Fig. 1. There were some missing data in all the stations so the comparison between the modeled DOD and AOD from Sun-photometers was not fully complete.

3.4 Satellite Data

The Moderate Resolution Imaging Spectro-radiometer (MODIS) aboard the Terra satellites passes north-south across the Equator in the morning, and Aqua satellites that pass south-north over the Equator in the afternoon. MODIS (Terra & Aqua) view the entire Earth's surface every one to two days. Its detectors measure 36 spectral bands between 0.405 and 14.385 μm , and it acquires data at three spatial resolutions: 250m, 500m, and 1,000m. Most Satellite sensors applied algorithms in order to retrieve AOD which is defined as the vertically integrated aerosol extinction and can be considered as an optical measure of the whole amount of aerosols (all types) with some wavelength dependence. MODIS comprises two aerosol algorithms, one used to derive the aerosols over land and the other used over ocean [46]. MODIS AOD algorithm over land works only over low ground reflectance (over dark vegetation). To calculate AOD over bright areas such as deserts, MODIS/Aqua-Deep Blue AOD product has been included in the analysis which provides information over arid and semi-arid areas and it is able to distinguish dust plumes from fine-mode pollution particles even in complex aerosol environments [47], [48]. The reliability and availability of MODIS AOD product in near real-time lead to a most widely use in aerosols studies. The advantages of using satellites data is the large spatial coverage and their availability in near real-time, while the including of all types of aerosols can limits the applications who involved in a particular aerosol type (like dust) which might be limited to seasons and regions in some cases, when or where that type dominates the aerosol composition [11].

A qualitative comparison between the dust loading from the BSC-DREAM8B V2.0 model and MODIS/Aqua images has been made to test the performance of the model and to describe the evolution of the dust plume over the area of study. Not all the images were used in the comparison because it is not matching the specified domain of the model that can't be good enough for the comparison. The Satellite images used in the comparison is not fitting the same timing of the dust loaded results but it was close to some extent. Another qualitative comparison has been made between MODIS/Aqua Ver. 5.1 (1°x1° Daily Level 3 data) which include Deep Blue AOD at 550 nm (over Land), AOD at 550 nm (over Ocean) and the modeled daily dust optical depth DOD at 550nm using BSC-DREAM8B V2 model for source mask extending below 35°N latitude or SM35 and source mask extending below 45°N latitude or SM45 and the calculated difference between both of them for the days of the case studies.

Table (2) Description of the selected AERONET stations including their longitude, latitude, elevation above sea level in meter with some information about their locations.

AERONET site	Longitude (° East)	Latitude (° North)	Elevation (m)	Site Location
Solar_Village	46.39729	24.90693	764.0	Inland Desert
KAUST_Campus	39.10283	22.30483	11.2	Urban , coastal
Nes_Ziona	34.78917	31.92250	40.0	Urban

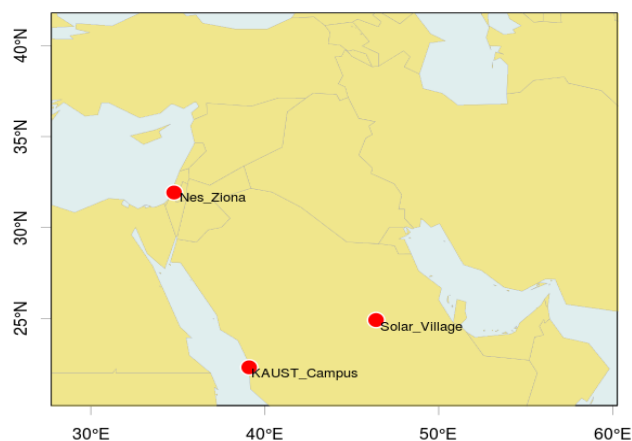


Fig. 1. The spatial distribution of the selected AERONET stations located within the study domain.

IV. Results and Discussion

4.1 The synoptic pattern for the dust study case

Fig. 2 shows the Sea level pressure from BSC-DREAM8b simulations and ERA-Interim reanalysis at 12:00 UTC from 1 to 4 June 2012, Fig. 3 shows the geopotential height from BSC-DREAM8b simulations and ERA-Interim reanalysis for the level 850 hPa at 12:00 UTC for the same days, Fig. 4 shows 10 m wind barbs in knots from BSC-DREAM8b simulations and ERA-Interim reanalysis at 12:00 UTC and Fig. 5 shows dust load from BSC-DREAM8b simulations for 1, 3 and 4 June at, 06:00 UTC, 09:00 UTC and Satellite images from MODIS/Aqua for 1, 3 and 4 June at 07:25 UTC, 10:25 UTC and 07:55 UTC respectively.

On 1 June, the model simulation of the upper air chart for 850 hPa shows low pressure systems with enclosed circulations centered over Iran, Turkey with a ridge over the Red Sea stretching easterly. This upper air disturbance leads to a significant pressure decrease in the lower atmosphere represented by a developed low-pressure system centered over south-western Iran stretching towards the north-west. Also, a ridge axis is seen over the eastern Mediterranean. This west – east synoptic systems lead to pressure gradients that generate a north-westerly airflow (summer Shamal) as shown in Fig. 4 where the north-westerly winds are observed over Syria and Iraq with highest wind speed over western Syria, southern Iraq, north and eastern parts of Saudi Arabia (KSA) that activated the dust sources in those regions as shown in Fig 7. In addition to this synoptic pattern, the effect of the terrain sloping to the west and south west in central KSA and the low elevations of the lower Tigris-Euphrates alluvial plain [49] helped in generating the north-westerly winds flow over the Arabian Gulf.

The next day, 850 hPa chart shows an intensification in the low pressure systems over Iran extending over eastern Iraq, while the ridge is seen extending eastward. The surface chart shows the domination of the low pressure pattern over Iran stretching towards the north-west over Syrian plateau and lower Tigris-Euphrates river basin that considered as potential dust sources as shown in Fig. 2. The wind speed was about 20 knots over western Iran and south-eastern Iraq and it blew dust towards the south east over the Arabian Gulf region and towards eastern KSA , a notable strong wind over Qatar was about 20 knots kicked up the dust which was transported towards the southeast.

The surface low pressure system become more intensified on 3 June over south-western parts of Iran extending toward the northwest (as well as in 850 hPa) affecting Iraq and the gulf region, this leads to increase the wind speed over central and southern Iraq, north and eastern KSA and the Arabian Gulf as shown in Fig. 4 Moreover, an intense ridge was over the Caspian Sea extending southward, this pressure gradient (clear in 850 hPa chart) strength the wind speed to reach 20 knots over northern Iran kicking up the dust over that region.

The surface low pressure pattern still dominating over Iran stretching north - westward on 4 June (also seen in the upper air chart) with a intense ridge axis over the Caspian Sea leading to activate dust sources in Iran while the north westerly wind about 10 knots is dominated over Iraq moving towards the Arabian Gulf region and the north-eastern parts of KSA.

BSC-DREAM8b Sea Level Pressure (hPa)

ERA Sea Level Pressure (hPa)

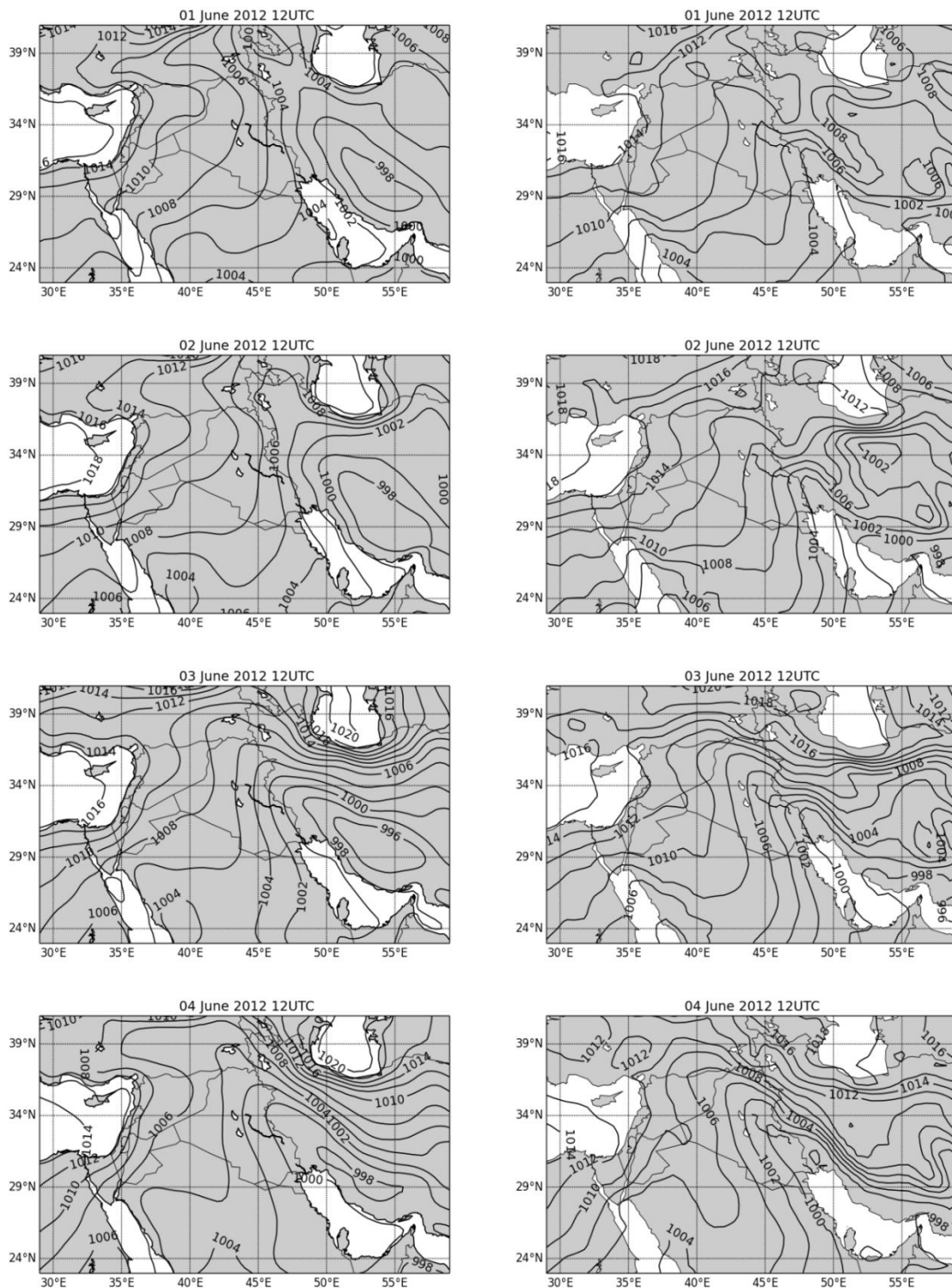


Fig. 2. Sea Level Pressure at 12:00 UTC from BSC-DREAM simulation (left) and ERA Interim at 12:00 UTC (right) for the days 1,2,3,4 June 2012.

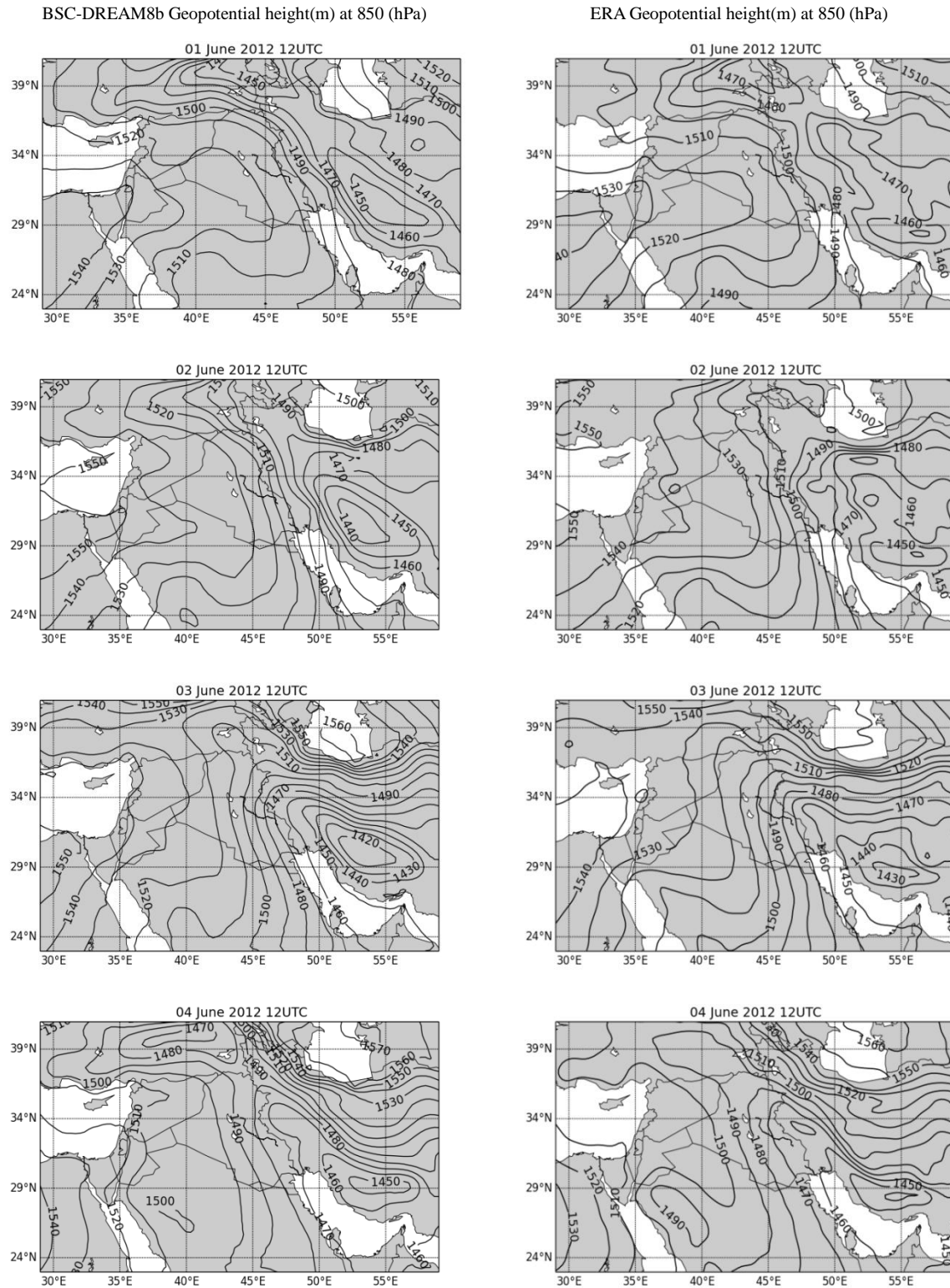


Fig. 3. Geopotential height (m) at 850 (hPa) at 12:00 UTC from BSC-DREAM simulation (left) and ERA Interim at 12:00 UTC (right) for the days 1,3,5,8 July 2009

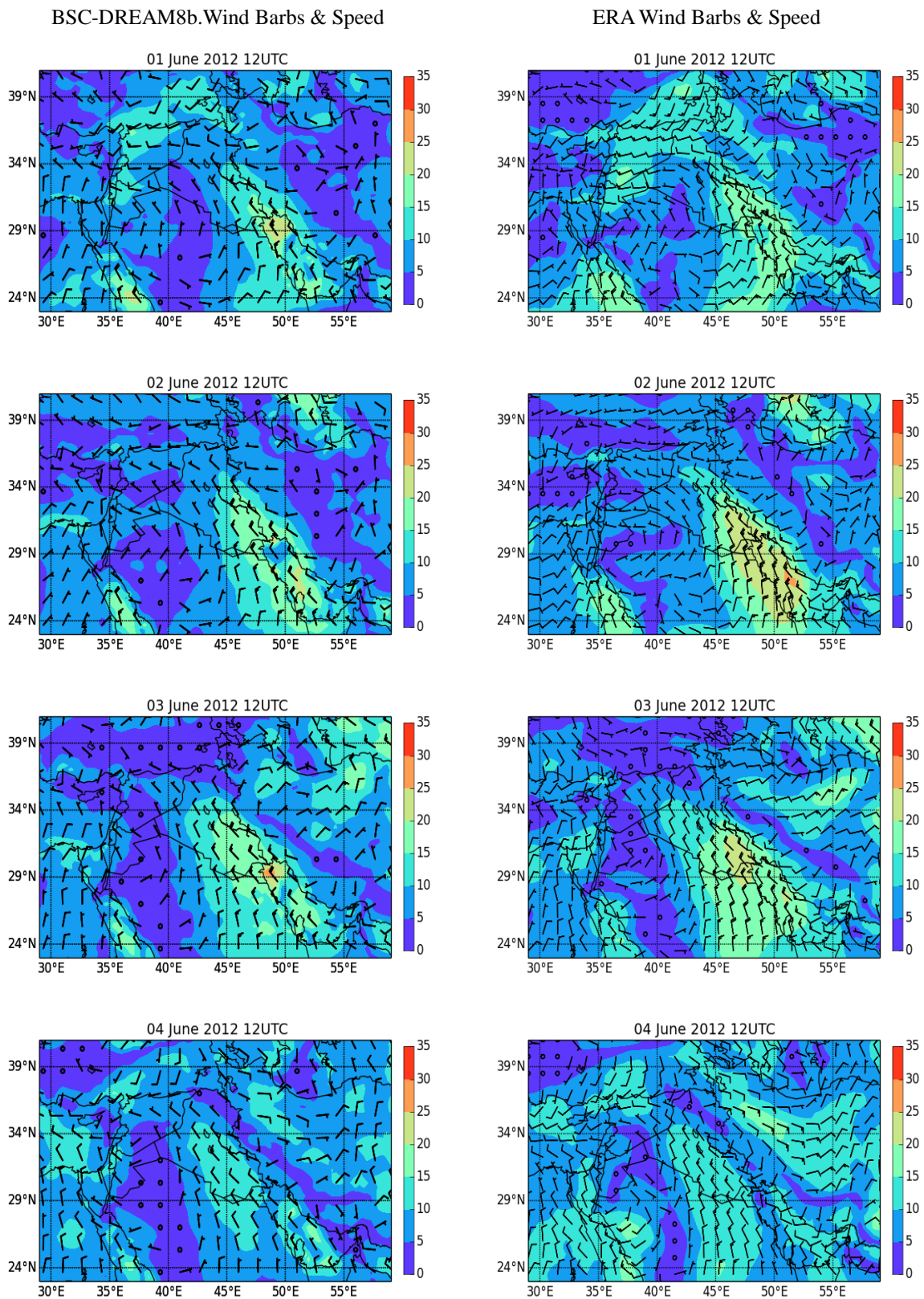


Fig. 4. Spatial distribution of 10 m wind barbs at 12:00 UTC using BSC-DREAM (left) and ERA Interim (right) for the days 1,2,3,4 June 2012.

The qualitative comparison between the dust loading from the BSC-DREAMv2 model and MODIS/Aqua satellite images show a good agreement between the spatial patterns of the dust plume and the corresponding satellite images as shown in Fig. 5.

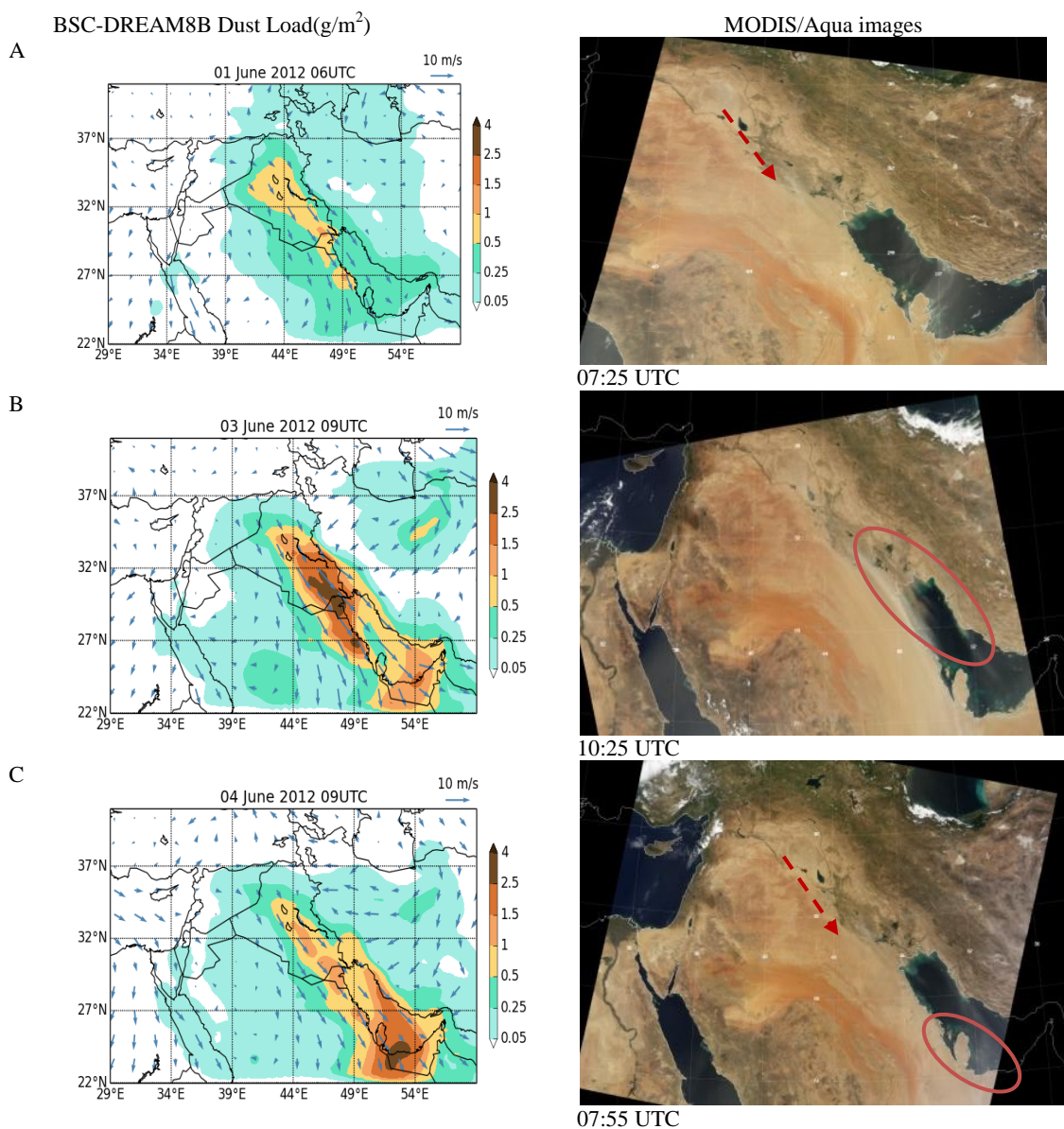


Fig. 5. BSC-DREAM8B Dust Load (g/m^2) (left), MODIS/Aqua images (right) for (A) 1 June, (B) 3 June, (C) 4 June 2012

4.2 Dust Optical properties

The variations in AOD during June, 2012 dust outbreak were tested using AERONET stations located in the Arabian Peninsula and eastern Mediterranean region within the study domain. They are Solar_Village, Kaust_Campus and Nes_Ziona.

Solar Village is located in the middle of the Arabian Peninsula, far from the Arabian Gulf or any industrial areas, thus it has a significant contribution of desert dust particles and it is considered as an inland desert site (as referred in Table 1). As shown in Fig. 6 A this site has a high aerosol loading (AOD) ranging between (0.3-1.8) with low values of Angstrom parameter ($\alpha < 0.3$) coincide to coarse mode of aerosols due to the existence of desert dust particles which is favorable in this season due to the dry weather condition in the Arabian Peninsula caused by Monsoon as referred by Liu et al. (2000) [50] and low humidity in that inland site. For this site, the model is able to simulate this event with almost similar behavior for DOD compared to AOD but in general there are underestimated values for the DOD for both types of extended source masks.

Kaust_campus is an urban and costal site at the shoreline of the Red Sea in the Arabian Peninsula, thus it is expected to find fine and coarse aerosols modes together in this site. According to Fig. 6B, the coarse mode

has the domination among fine mode with high aerosol loading especially on the first three days of June with maxima of 1.7 and low values for the Angstrom parameter $\alpha \sim 0$. This may denote to existence of desert dust particles and/or sea spray particles due to the proximity of this site to the sea. The results of the model have zero and close to zero values of the modeled DOD for both source mask extensions which denotes that there is a trace of dust. In coastal sites, the interaction of mineral dust and pollutants is strong. Under high relative humidity conditions, aged dust aerosols are often coated with soluble materials such as sulphate as referred by Dentener et al. (1996) [51] which can interpret the high value of AOD and low values of Angstrom parameter. Another probable reason is that soluble particles such as sulphates grow in size under high relative humidity and these increases AOD values and decrease Angstrom parameter values due to the enlargement of the soluble particles according to Levin et al. (1996) [52].

In contrast to Kaust_Campus site, the fine mode has the domination in Nes_Ziona station as shown in figure (6 C). The station is an urban and coastal site located in the Eastern Mediterranean, with high values of Angstrom parameter ($\alpha > 0.5$) and maxima of 1.4 corresponding to low values of aerosol dust loading (AOD < 0.4) which is coincide to pollutants due to emissions from urban and industrial activities (anthropogenic aerosols). The absence of wet removal mechanisms in this season made the contribution of pollutants in its maximum as referred by Basart (2011) [53]. Due to the absence of dust in that site, the model calculated DOD with zero values for both types of source masks; this is a good indicator for the use of the model as a tool to separate the dust from the anthropogenic effect in the measurements of the Sun-photometers.

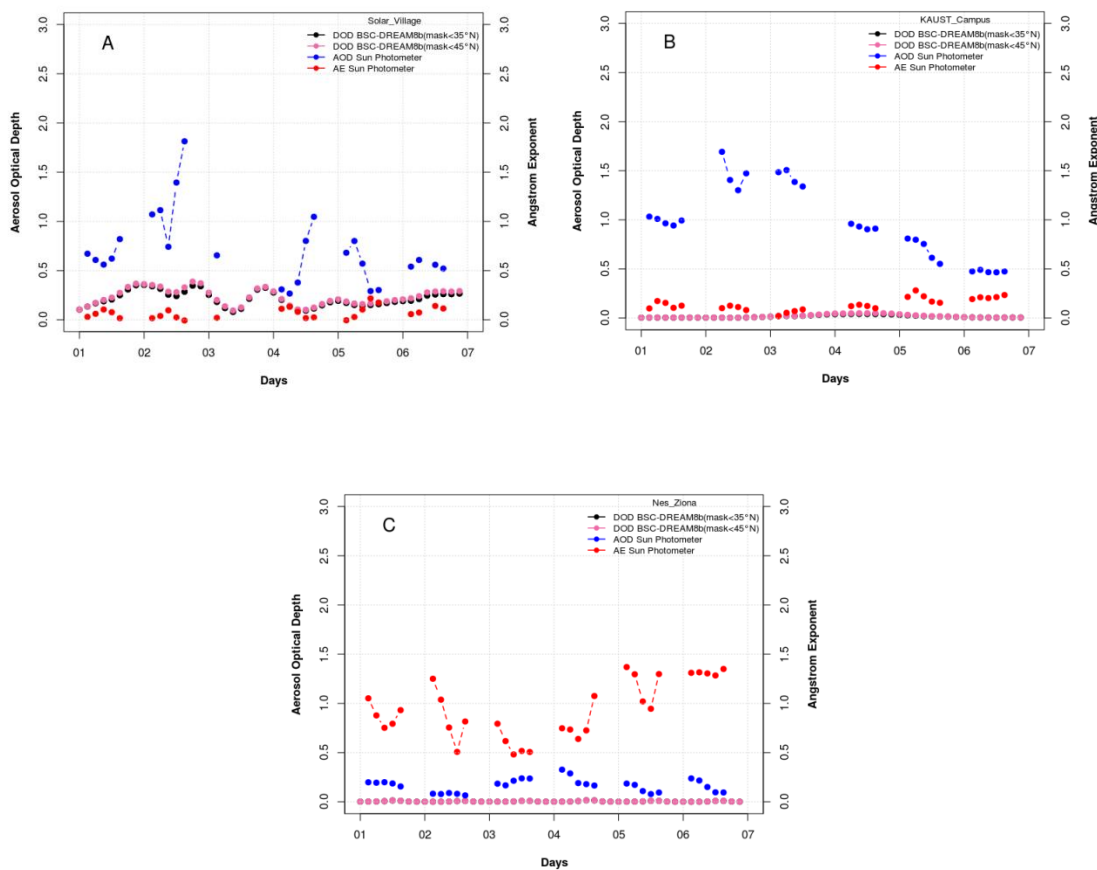


Fig. 6. Time series for Dust optical Depth DOD at 550 nm using BSC-DREAM8b model (black line) with source mask extended below 35° N latitude and below 45° N latitude (pink line) and Aerosol Optical Depth (AOD) measurements from sun-photometers (blue line) and Angstrom parameter calculated between 440 and 870 nm (red line) for the stations of (A) Solar village, (B) Kaust_Campus, (C) Nes_Ziona

The Ground-based instruments can be used to measure AOD in the atmosphere above the location of the instrument only, while the satellite sensors provide a view of AOD over a large area, in addition to the lack of continuous dust observations for many remote areas which can be provided only by Satellite sensors, thus Satellite sensor data from the Moderate Resolution Imaging Spectro-radiometer (MODIS) is used in this study.

Fig.7 shows MODIS products of AOD and the model products of DOD for the two source mask extensions and the resulted difference of using both of them for the period 1-6 June 2012.

on 1 June, the north-westerly wind provoked the dust from the sources in eastern Syria, the Syrian-Iraqi borders and Tigris-Euphrates basin in Iraq towards southeast, over the Arabian Gulf, western Iran and into north-eastern Saudi Arabia where the dust source in Ad-Dahna Desert is activated, a central division of the Arabian Desert, which considered as a potential dust source in the Arabian Peninsula as shown in MODIS map. The model is consistent with MODIS over parts of the source regions while it underestimated the AOD over the other regions in Saudi Arabia and Iraq.

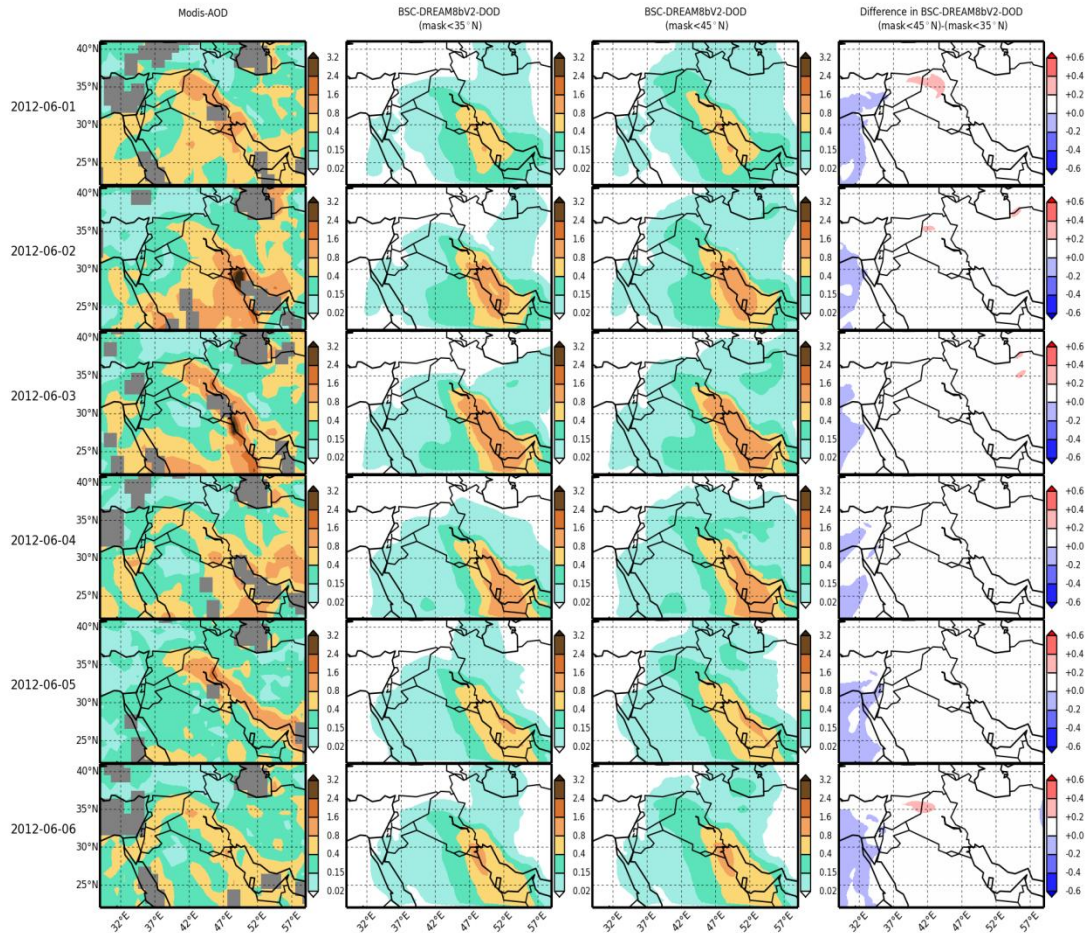


Fig. 7 MODIS/Aqua daily AOD at 550 nm (over Land and Ocean), Dust optical Depth (DOD) at 550nm using BSC-DREAM8b model with source mask < 35 latitude, and source mask < 45 latitude and the difference between both for the days (1-6) June 2012

The next two days MODIS maps shows the advection of dust down to Arabian Gulf region causing an extensive dust load over Kuwait and its borders with Saudi Arabia with AOD values oscillating between 2.4 to 3.2, the dust transported also to the southwest and southeast of Iraq towards north-eastern parts of Saudi Arabia and western parts of Iran respectively while the model worked with underestimation over those regions on 2 June and overestimation over UAE and the north-eastern parts of the Arabian Gulf on the 3 June. Also, a notable dust plume over central Iran and the Caspian Sea is shown in which this region witness dust events peaking in June and July while the model missed out the dust over that region and underestimated the dust load over Syria and northern parts of Iraq.

The dust episode continued for the next three days with the same transport patterns. In general the model worked in compatibility with MODIS over southern Iraq and the Gulf Region on 4 and 6 of June with overestimation on 5 June, while the model results indicate to a disagreement with MODIS for the other regions of the domain because of the underestimated values of AOD.

Using SM45 enhanced the dust emissions due to the inclusion of more dust sources and hence it gave higher values for the AOD for source regions located above 35°N latitude, while it gave a similar pattern of the dust transport which obtained by using SM35.

It is obvious that there is a difference between the AOD from MODIS and DOD from the model. One of the reasons behind this is that MODIS includes all the type of Aerosols (fine and coarse) while the model calculates the dust only. Another reason could be related to the underestimated values of wind speed over some dust source regions as it shown in figure 4 which affect the performance of the model in generating dust, but in general the model succeeded in presenting a clear pattern of dust that extended from the northern part of the Tigris-Euphrates basin to the Arabian Gulf region which is considered as the sources of dust in the Middle East as it referred by Prospero et al. (2002) [4].

The difference between the AOD values by using SM35 and SM45 shows positive values over Syrian - Iraqi borders on 1, 2, 6 June in addition to northern Iraq on 1 June, this is due to include more dust sources in SM45 that lead to generate more dust. While increasing dust-loaded gives negative values over eastern Mediterranean and Egypt for all days due to dust radiative effect leading to generate less amount of dust as it referred by Miller et al. (2004) [54].

V. Conclusions

In the first days of June, a dust storm struck Iraq, Kuwait, Qatar and north-eastern parts of Saudi Arabia due to the to the domination of low pressure system over Iran and the Arab gulf region and high pressure cells placed over the north of Africa and south of Mediterranean Sea. Syria and Iraq have the main contribution in emitting dust to their neighbors in which the north-westerly wind (Summer Shamal) transporting the dust across the Tigris and Euphrates river valleys of Iraq towards the southeast, southwest and east to Arabian Gulf region, north-eastern KSA and western Iran.

Comparing the model simulation at the surface with ERA-Interim reanalysis data resulted in compatibility between both and showing the same synoptic patterns especially for 3 and 4 of June and with some shifting in the trough axis towards the west for 1 and 2 June. The model results for the geopotential heights at 850 hPa are corresponded well with the ERA-I reanalysis, it shows the same synoptic patterns over the region of study for all the tested days. The comparison between the wind direction and speed between both sets of data shows a high compatibility in simulating the wind direction for the tested days, and good results for the wind speed with some underestimation in eastern KSA for all the days; western parts of Syria, south-eastern Iraq and the red sea on the 1 June; south of Iraq and over the Arabian Gulf on 2 June; southern of Iraq on 3 June; northern parts of the Red Sea and central Iran on 4 June; and overestimation on 1 and 2 of June over northern Arabian Gulf.

The spatial patterns of the dust plume show a good agreement with the corresponding satellite images suggesting that the model is able to predict the dust event and succeeded in simulating the movement of dust plume.

Comparing the simulated DOD with AERONET AOD observations for inland, urban and costal, and urban stations shows the ability of the model to simulate the dust events when the dominated type of aerosols is desert dust but with underestimated values for the DOD by using both types of extended source masks, and with zero values for the dust optical depth when the dominated aerosols mode are fine. Thus the model can be used as a tool to separate dust from the anthropogenic effect in the measurements of the Sun-photometers.

The model is consistent with MODIS over parts of the source regions in Syria, Iraq and north-eastern Saudi Arabia but it worked with underestimation especially over central Saudi Arabia and Iraq, with overestimation over UAE and the north-eastern parts of the Arabian Gulf on the 3,5 June. While the model missed out the dust over central Iran and the Caspian Sea and underestimated the dust load over Syria and northern parts of Iraq. In general the model succeeded in simulating the activation of dust sources in Syria, Iraq, areas in Kuwait, UAE, Iran and eastern KSA but it missed out the activation of dust sources in southern KSA. In general DOD values were underestimated compared to MODIS AOD in which the latter includes all types of aerosols while the model computed the dust only. Using the source mask SM45 improved the values of the DOD and gave higher values with the same behaviour. The difference between the AOD values by using SM35 and SM45 shows positive values over Syrian - Iraqi borders and northern Iraq due to include more dust sources in SM45 that lead to generate more dust. While increasing dust-loaded gives negative values over eastern Mediterranean and Egypt due to dust radiative effect leading to generate less amount of dust.

Acknowledgment

The authors would like to thank Barcelona Supercomputing Center, Earth Science department staff for their valuable help and support especially Jose M. Baldasano, Sara Basart, Kim Serradel and Francesco Benincasa. Also, to AERONET program for maintaining and offering the data.

References

- [1] IPCC, Intergovernmental Panel on Climate Change, 2001: Climate change 2001: The Scientific Basis. Contribution of Working Group I to the Third Assessment Report of the Intergovernmental Panel on Climate Change (CAMBRIDGE UNIVERSITY PRESS, 2001).

- [2] P. Knippertz and J. W. Stuut, *Mineral Dust A Key Player in the Earth System* (Springer Dordrecht Heidelberg New York London, 2014).
- [3] J. E. Penner, M. Andreae, H. Annegarn, L. Barrie, J. Feichter, D. Hegg, A. Jayaraman, R. Leaitch, D. Murphy, J. Nganga and G. Pitari, *Aerosols, Their Direct and Indirect Effects. Climate Change 2001: The Scientific Basis. Contribution of Working Group I to the Third Assessment Report of the Intergovernmental Panel on Climate Change* (C. A. Johnson. Cambridge, New York, Cambridge University Press, 2001) 289-348.
- [4] J. M. Prospero, P. Ginoux, O. Torres, S. E. Nicholson, and T. E. Gill, *Environmental characterization of global sources of atmospheric soil dust identified with the nimbus 7 total ozone mapping spectrometer (TOMS) absorbing aerosol product*, *Rev. Geophys.*, 40(1), 2002,2-1–2-31.
- [5] A. D. Bolorani, S.O. Nabavi, R. Azizi and H.A. Bahrami, *Characterization of dust storm sources in western Iran using a synthetic approach*, in C. Helmis, and P. T. Nastos (Ed.), *Advances in Meteorology, Climatology and Atmospheric Physics* (Springer Atmospheric Sciences,2013) 415-420.
- [6] P. Ginoux, J.M. Prospero, T.E. Gill, N.C. Hsu, and M. Zhao M ,*Global-scale attribution of anthropogenic and natural dust sources and their emission rates based on MODIS Deep Blue aerosol products*, *Rev Geophys* 50(RG3005), 2012, 1-36 (doi:10.1029/2012RG000388).
- [7] WMO, UNEP, *Establishing a WMO sand and dust storm warning advisory and assessment system regional node for West Asia: current capabilities and needs* (WMO, 2013).
- [8] S. Nickovic, G. Kallos, A. Papadopoulos, and O. Kakaliagou, *A model for prediction of desert dust cycle in the atmosphere*. *J Geophys Res*, 106(D16), 2001, 18113–18130.(doi:10.1029/2000JD900794).
- [9] C. Pérez, S. Nickovic, G. Pejanovic, J. M. Baldasano, and E. Ozsoy, *Interactive dust-radiation modeling: a step to improve weather forecasts*. *J Geophys Res*, 111(D16206), 2006a,1-17 (doi:10.1029/2005JD006717).
- [10] Pérez C., S. Nickovic, J. M. Baldasano, M. Sicard, F. Rocadenbosch, and V. E. Cachorro, *A long Saharan dust event over the western Mediterranean: Lidar, sun photometer observations, and regional dust modeling*. *J Geophys Res*, 111(D15214), 2006b, 1-16 (doi:10.1029/2005JD006579).
- [11] S. Basart, C. Pérez, S. Nickovic, E. Cuevas, and J. M. Baldasano, *Development and evaluation of the BSC-DREAM8b dust regional model over Northern Africa, the Mediterranean and the Middle East*, *Tellus B* 64(18539),2012a,1-23. <http://dx.doi.org/10.3402/tellusb.v64i0.18539>
- [12] K. Haustein, C. Pérez, J. M. Baldasano, D. Müller, M. Tesche, A. Schladitz, M. Esselborn, B. Weinzierl, K. Kandler, and W. V. Hoyningen-Huene, *Regional dust model performance during SAMUM 2006*, *J. Geophys. Res. Lett.*, 36(L03812), 2009, 1-6(doi: 10.1029/2008GL036463).
- [13] D. K. Papanastasiou, A. Poupkou, E. Katragkou, V. Amiridis, D. Melas, N. Mihalopoulos, S. Basart, C. Pérez, and J. M. Baldasano, *An Assessment of the Efficiency of the Dust Regional Modelling to Predict Saharan Dust Transport Episodes*, *Advances in Meteorology*, 154368, 2010, 1-9 (doi:10.1155/2010/154368).
- [14] M. T. Pay, M. Piot, O. Jorba, S. Gassó, M. Gonçalves, S. Basart, D. Dabdub, P. Jiménez-Guerrero, and J. M. Baldasano, *A Full Year Evaluation of the CALIOPE-EU Air Quality Modeling System over Europe for 2004*, *Atmos. Environ.*, 44(27), 2010, 3322-3342, (doi:10.1016/j.atmosenv.2010.05.040).
- [15] S. Basart, M. T. Pay, O. Jorba, C. Pérez, P. Jiménez-Guerrero, M. Schulz, and J. M. Baldasano, *Aerosols in the CALIOPE air quality modelling system: evaluation and analysis of PM levels, optical depths and chemical composition over Europe*. *Atmos Chem Phys* 12(3363–3392), 2012b (doi:10.5194/acp-12-3363-2012).
- [16] M. T. Pay, P. Jiménez-Guerrero, O. Jorba, S. Basart, X. Querol, M. Pandolfi, and J. M. Baldasano, *Spatio-temporal variability of concentrations and speciation of particulate matter across Spain in the CALIOPE modeling system*, *Atmos. Environ.*, 46, 2012, 376–396 (doi:10.1016/j.atmosenv.2011.09.049).
- [17] F. Mesinger, Z. I. Janjic, S. Nickovic, D. Gavrilo, and D. G. Deaven, *The step-mountain coordinate: model description, and performance for cases of Alpine lee cyclogenesis and for a case of an Appalachian redevelopment*. *Mon Weather Rev* 116(7), 1988, 1493–1518.
- [18] Z. I. Janjic, *The Step-mountain Eta Coordinate Model: Further developments of the convection, viscous sublayer and turbulence closure schemes*, *Mon. Weather Rev.*, 122, 1994, 927– 945.
- [19] Q. Zhao and F. H., Carr, *A prognostic cloud scheme for operational NWP models*, *Mon. Weather Rev.*, 125, 1997,1931- 1953.
- [20] S. Nickovic, and S. Dobricic, *A model for long-range transport of desert dust*. *Mon Weather Rev*124, 1996, 2537–2544.
- [21] I. Tegen, S.P. Harrison, K.E. Kohfeld, I.C. Prentice, M.C. Coe and M. Heimann, *The impact of vegetation and preferential source areas on global dust aerosol: results from a model study*, *J. Geophys. Res.*, 107(D21), 2002, 14-1–14-21(doi:10.1029/2001JD000963).
- [22] J. L. Dorman and P. J. Sellers, *A Global Climatology of Albedo, Roughness Length and Stomatal Resistance for Atmospheric General Circulation Models as Represented by the Simple Biosphere Model (SiB)*, *Journal of Applied Meteorology*, 28, 1989, 833-855.
- [23] B. Staub and C. Rosenzweig, *Global digital data sets of soil type, properties: documentation of archived data tape* (United States. Goddard Institute for Space, 1987).
- [24] FAO, *FAO/UNESCO Soil map of the world*. Technical report (ISRIC,Wagneingen, 1988).
- [25] D. Hillel, *Introduction to Soil Physics* (Academic, San Diego, Calif, 1982).
- [26] B.J. Cosby, G.M. Hornberger, R.B. Clapp, and T.R. Ginn, *A statistical exploration of the relationship of soil moisture characteristics to the physical properties of soils*, *Water Resources Research* 20 (6), 1984, 682-690.
- [27] P. Ginoux, M. Chin, I. Tegen, J. M. Prospero, B. Holben, O. Dubovik and S.-J. Lin., *Sources and distributions of dust aerosols simulated with the GOCART model*, *Geophys. Res.* 106(D17), 2001, 20255-20274.
- [28] G. A. D'Almeida, *On the variability of desert aerosol radiative characteristics*, *JGR. Journal of geophysical research. Part D, Atmospheres*, 92(3), 1987, 3017-3026.
- [29] Y. Shao, M.R. Raupach, and P.A. Findlater, *Effect of Saltation Bombardment on the Entrainment of Dust by Wind*", *J. Geoph. Res.* 98(D7), 1993, 12719–12726.
- [30] R. A. Bagnold, *The Physics of Blown Sand and Desert Dunes* (Morrow, New York, 1941).
- [31] B. R. White, *Soil transport by winds in Mars*, *J. Geophys. Res.*, 84, 1979, 4643-4651.
- [32] F. Fecan, B. Marticorena, and G. Bergametti, *Parameterization of the increase of the Aeolian erosion threshold wind friction velocity due to soil moisture for arid and semi-arid areas*, *Annales Geophys.*, 17(1), 1999, 194-157.
- [33] G. Bergametti, L. Gomes, G. Coudé-Gaussen, P. Rognon, M-NL Coustumer, *African dust observed over Canary Islands: source-regions identification and transport pattern for some summer situations*, *J Geophys Res* 94, 1989,14855–14864

- [34] L. Zhang, S. Gong, J. Padro, and L. Barrie, *A size-segregated particle dry deposition scheme for an atmospheric aerosol module*, *Atmos. Environ.*, **35**, 2001,549-560.
- [35] W. G. N. Slinn, *Predictions for particle deposition to vegetative canopies*, *Atmos. Environ.*, **16**, 1982, 1785-1794.
- [36] C. Zender, H. Bian, and D. Newman, *Mineral Dust Entrainment and Deposition (DEAD) model: Description and 1990s dust climatology*, *Geophys. Res.*, **108(D14)**, 2003, 8-1– 8-19.
- [37] E.P. Shettle, *Optical and radiative properties of a desert aerosol model*, in G. Fiocco (Eds.), *Proceedings of the Symposium on Radiation in the Atmosphere* (A. Deepak Publishing, Hampton, Va.,1984) 74- 77.
- [38] M. Schulz, Y.J., Balkanski, W. Guelle, and F. Dulac, *Role of aerosol size distribution and source location in a three-dimensional simulation of a Saharan dust episode tested against satellite-derived optical thickness*, *J.Geoph. Res.* **103(D9)**, 1998, 10579- 10592.
- [39] M. I. Mishchenko, L. D., Travis, and A. A. Lacis, *Scattering, Absorption, and Emission of Light by Small Particles* (Cambridge Univ. Press, Cambridge, 2002).
- [40] M. I. Mishchenko, J. W., Hovenier, and L. D. Travis, *Light Scattering by Nonspherical Particles* (Springer, New York, 2000).
- [41] A. A. Lacis, and M. I., Mishchenko, *Climate forcing, climate sensitivity, and climate response: A radiative modeling perspective on atmospheric aerosols*, in R. J. Charlson and J. Heintzenberg, *Aerosol Forcing of Climate, Report of the Dahlem Workshop on Aerosol Forcing of Climate*, Berlin 1994, April 24– 29 (John Wiley, Hoboken, N. J. ,1995).
- [42] I. Tegen, A. A. Lacis, and I. Fung, *The influence on climate forcing of mineral aerosols from disturbed soils*. *Nature* **380**, 1996, 419–422.
- [43] D. P. Dee, S. M. Uppala, A. J. Simmons, P. Berrisford, P. Poli, S. Kobayashi, and U. Andrae et al. , *The ERA-Interim reanalysis: Configuration and performance of the data assimilation system*. *Quarterly Journal of the Royal Meteorological Society*, **137(656)**, 2011, 553-597(doi:10.1002/qj.828).
- [44] B.N. Holben, T.F. Eck, I. Slutsker, D. Tanré, J. P. Buis, A. Setzer, E. Vermote, J. A. Reagan, Y. Kaufman, T. Nakajima, F. Lavenu, I. Jankowiak, and A. Smirnov, *AERONET – a federated instrument network and data archive for aerosol characterization*. *Remote Sens Environ* **66**, 1998, 1–16.
- [45] T. F. Eck, B. N. Holben, J. S. Reid, O. Dubovik, A. Smirnov, N. T., O’Neill, I. Slutsker, and S. Kinne, *Wavelength dependence of optical depth of biomass burning, urban and desert dust aerosols*, *J.Geophys. Res.*, **104(D24)**, 1999, 31333-31350.
- [46] L. A. Remer, Y. J. Kaufman, D. Tanré, S. Mattoo, D. A. Chu, J. V. Martins, R. R. Li, C. Ichoku, R.C. Levy, R. G. Kleidman, T. F. Eck, E. Vermote, and B. N. Holben, *The MODIS Aerosol Algorithm, Products, and Validation*, *J. Atmos. Sci.*, **62**, 2005,947-973.
- [47] N. C. Hsu, S. C. Tsay, M. King, and J. R. Herman, *Aerosol properties over bright-reflecting source regions*. *IEEE Trans. Geosci. Remote Sens.*, **42**, 2004,557 – 569.
- [48] N. C. Hsu, S.-C. Tsay, King, and M. D. Herman JR, *Deep Blue retrievals of Asian aerosol properties during ACE-Asia*. *IEEE Trans Geosci Remote Sens* **44(11)**,2006,3180–3195.
- [49] P. G. Rao, M. Al-Sulaiti, and A. H. Al-Mulla, *Winter shamals in Qatar, Arabian Gulf*. *Weather*, **56**, 2001, 444-451.
- [50] M. Liu, D. L. Westphal, T. R. Holt, and Q. Xu, *Numerical Simulation of a Low-Level Jet over Complex Terrain in Southern Iran*, *Mon. Weather Rev.*, **128(5)**, 2000, 1309-1327.
- [51] F.J. Dentener, G. R. Carmichael, Y. Zhang, J. Lelieveld, and P. J. Crutzen , *Role of mineral aerosol as a reactive surface in the global troposphere*. *J Geophys Res* **101(D17)**, 1996, 22869–22889.
- [52] Z. Levin, E. Ganor, and V. Gladstein, *The effects of desert particles coated with sulphate on rain formation in the eastern Mediterranean*. *J Appl Meteorol* **35**, 1996, 1511–1523.
- [53] S. A. Basart, *Desert dust characterization in North Africa, Middle East and Europe through regional dust modeling, and satellite-borne and ground based observations*. Ph.D. Thesis, Spain, UNIVERSITAT POLITÈCNICA DE CATALUNYA, 2011.
- [54] R. L. Miller, I. Tegen, and J. Perlwitz, *Surface radiative forcing by soil dust aerosols and the hydrologic cycle*. *J Geophys Res* **109**, D04203, 2004b, 1-24 (doi: 10.1029/2003JD004085).